Spontaneous vasomotion propagates along pial arterioles in the awake mouse brain like stimulus-evoked vascular reactivity

Leon P Munting[1] , **Orla Bonnar**[1] , **Mariel G Kozberg**[1,2],
Corinne A Auger[1], **Lydiane Hirschler**[2,3] , **Steven S Hou**[1],
Steven M Greenberg[2], **Brian J Bacskai**[1] and **Susanne J van Veluw**[1,2]

Abstract
Sensory stimulation evokes a local, vasodilation-mediated blood flow increase to the activated brain region, which is referred to as functional hyperemia. Spontaneous vasomotion is a change in arteriolar diameter that occurs without sensory stimulation, at low frequency ($\sim$0.1 Hz). These vessel diameter changes are a driving force for perivascular soluble waste clearance, the failure of which has been implicated in neurodegenerative disease. Stimulus-evoked vascular reactivity is known to propagate along penetrating arterioles to pial arterioles, but it is unclear whether spontaneous vasomotion propagates similarly. We therefore imaged both stimulus-evoked and spontaneous changes in pial arteriole diameter in awake, head-fixed mice with 2-photon microscopy. By cross-correlating different regions of interest (ROIs) along the length of imaged arterioles, we assessed vasomotion propagation. We found that both during rest and during visual stimulation, one-third of the arterioles showed significant propagation (i.e., a wave), with a median (interquartile range) wave speed of 405 (323) μm/s at rest and 345 (177) μm/s during stimulation. In a second group of mice, with GCaMP expression in their vascular smooth muscle cells, we also found spontaneous propagation of calcium signaling along pial arterioles. In summary, we demonstrate that spontaneous vasomotion propagates along pial arterioles like stimulus-evoked vascular reactivity.

Introduction

Local increases in cerebral blood flow in response to neuronal activation are referred to as functional hyperemia and rely on neurovascular coupling (NVC).[1] As a result of the local increase of oxygenated blood out of proportion to the consumption of oxygen, the concentration of deoxyhemoglobin decreases locally, which forms the basis for detection of activated brain areas with imaging techniques such as blood oxygenation level dependent (BOLD)-fMRI[2] and optical intrinsic signal imaging.[3] To evoke neuronal activation in such imaging studies, participants are frequently subjected to sensory or motor stimulation paradigms. A widely used example is visual stimulation – during which the participant is presented with a screen displaying a flashing checkerboard – leading to activation of neurons in the visual cortex and ensuing stimulus-evoked vascular reactivity (i.e., functional hyperemia). Motor tasks such as finger tapping can also be used to evoke NVC in the motor cortex.[4]

[1]MassGeneral Institute for Neurodegenerative Research, Massachusetts General Hospital, Charlestown Navy Yard, MA, USA
[2]J. Philip Kistler Stroke Research Center, Massachusetts General Hospital, Boston, MA, USA
[3]C. J. Gorter Center for High Field MRI, Department of Radiology, Leiden University Medical Center, Leiden, the Netherlands

Corresponding author:
Susanne J van Veluw, MassGeneral Institute for Neurodegenerative Disease, Massachusetts General Hospital, 114 16th Street, Charlestown, MA 02129, USA.
Email: svanveluw@mgh.harvard.edu

Mechanistically, these blood flow increases are mediated by the relaxation of contractile mural cells, which results in an increase of the vessel diameter. After neuronal activation, the signal to dilate is propagated upstream along penetrating to surface arterioles, commonly referred to as pial or leptomeningeal arterioles.[5,6] Upstream stimulus-evoked vasodilation propagation has been observed both with intravital microscopy[7–9] and with BOLD-fMRI.[9]

Vessel diameter changes have also been observed without evoking neuronal activity. These spontaneous vessel diameter changes are referred to as vasomotion and occur at low frequency, generally around 0.1 Hz.[10] Vasomotion occurs spontaneously in isolated arterioles,[11] but can be entrained in cerebral vessels by neuronal activity.[12] Vasomotion has also been observed in other organs than the brain, including the skin[13] and the mesentery.[14] Furthermore, vasomotion has been observed across species, such as in awake mice with 2-photon microscopy[15] and in humans undergoing brain surgery.[16] Together with cardiac and respiratory fluctuations, vasomotion has been shown to drive flow of cerebrospinal fluid (CSF) in the perivascular spaces.[15,17,18] These spaces form important drainage pathways for clearance of metabolic waste from the brain extracellular space.[19] Failure of perivascular clearance is implicated in pathologic protein accumulation in neurodegenerative diseases, such as Alzheimer's disease (AD) and cerebral amyloid angiopathy (CAA).[20] We previously found that perivascular clearance can be enhanced by driving vessel diameter changes at the vasomotion frequency with visual stimulation in awake mice.[15] The exact mechanisms of vasomotion-mediated clearance are however still unclear. Previous modeling work suggests that an outward flow could be created if vasomotion waves travel upwards to the brain surface, against the direction of blood flow.[21] It is still unclear however, whether vasomotion indeed propagates along cortical arterioles *in vivo*.

Here, we use 2-photon microscopy in awake, head-fixed mice to detect vasomotion and compare its properties to visually-evoked vascular reactivity (i.e., functional hyperemia). We use plasma-labeling and genetically encoded calcium indicators expressed by mural cells, to measure the vessel diameter and to visualize changes in calcium concentration in individual vascular smooth muscle cells (VSMCs), which ultimately determines smooth muscle cell tone.[5] By cross-correlating different segments along the imaged arterioles, we found that spontaneous vasomotion indeed propagates along pial arterioles, with similar properties as stimulus-evoked vascular reactivity.

Materials and methods

Animals

The first cohort consisted of a group of 7 male C57Bl/6J mice that were ordered from the Jackson Laboratory (Bar Harbor, ME, USA), stock number 000664. They were imaged at the age of 4–6 months. An additional single C57Bl/6J mouse was imaged at 5 months of age for the data in supplementary figure 1. Furthermore, a second cohort of mice was used, which consisted of 5 transgenic mice (4 females) that express a genetically-encoded calcium indicator (GCaMP6f) in VSMCs and pericytes. They were imaged at the age of 6–10 months and were on a mixed background (C57Bl/6J and FVB). The mice were obtained by crossing the Ai95 mouse (stock number 028865) of the Jackson Laboratory (C57BL/6J background), which expresses GCaMP6f after Cre exposure, with a transgenic mouse that expresses Cre under the platelet-derived growth factor receptor-β (PDGFR-β) promotor[22] (FVB/NJ background). The latter mouse was a kind gift from Dr. Andy Shih from the Seattle Children's Research Institute. Small sample sizes were used, because of the exploratory nature of the study, where the intention was to collect basic evidence for propagation of vasomotion along cortical arterioles. Mice were housed in groups of up to four littermates on a 12 h day/night circle in individually ventilated cages supplied with bedding, unlimited chow food, and water. After cranial window surgery, the mice were housed individually.

All experiments were approved by the Massachusetts General Hospital Animal Care and Use Committee under protocol number 2018N000131. The studies were compliant with the National Institutes of Health Guide for the Care and Use of Laboratory Animals. Reporting of this study was in compliance with the ARRIVE guidelines.[23]

Surgery

The cranial window procedure employed has been described before.[15,24] In short, mice were anesthetized with isoflurane anesthesia in pure oxygen (induction at 5% and maintenance at 1.8–2.0%). They were then placed in a stereotactic frame, and the scalp skin was disinfected and subsequently removed to expose the skull. After craniotomy, a cover glass was positioned over the exposed cortex and sealed with a 1:1 mix of dental cement and KrazyGlue. Thereafter, a customized headpost made of stainless steel (Ponoko) was fixed to the skull with C&B Metabond (Parkell), to facilitate head fixation for awake imaging. The mice in the first cohort underwent a craniotomy at the

level of the right visual cortex (1.5 mm lateral and 1 mm caudal from lambda), with a diameter of 3 mm, allowing to study vascular responses to visual stimulation. Since mice on an FVB background are born blind, the window in the second cohort of mice was placed over the bilateral somatosensory cortices (spanning from 1 mm rostral of bregma to 1 mm caudal from lambda, 0 mm lateral), with a diameter of 5 mm, allowing to study vascular responses to whisker stimulation.

2-Photon microscopy

Mice were given at least 3 weeks of recovery time after surgery and before imaging. Each mouse from the first cohort underwent three awake imaging sessions, during day-time, with 2 weeks in between the sessions. Before imaging, the mice were briefly anesthetized with isoflurane to intravenously (i.v.) administer 200 μL of 70 kDa fluorescein-labeled dextran (2 mg/mL in sterile PBS; Invitrogen). Thereafter, they were head-fixed and allowed to freely walk on a circular treadmill placed under the microscope objective. To limit the potential effect of the brief isoflurane exposure (to administer i.v. dextran) on hemodynamics, we waited to start the experiment until the mice were fully active again. Imaging was performed with a FluoView FV1000MPE 2-photon laser scanning system (Olympus) with a Mai Tai® DeepSee™ Ti:Sapphire laser (Spectra-Physics), installed on a BX61WI Olympus microscope with a 25X, 1.05 NA objective. Emission light was detected with two photomultiplier tubes (Hamamatsu) after filtering out green (495–540 nm) light, and in cohort 2 also red (575–630 nm) light. The laser power was optimized per imaging session, but detector sensitivity settings were kept constant.

First, a middle-caliber pial arteriole ($\sim$20 μm) was identified through the eyepiece. Arterioles could be readily distinguished from a venule by their morphology and the ability to exhibit spontaneous dilations. After acquisition of a 200–300 μm Z-stack centered around that arteriole, and unless indicated otherwise, the following imaging parameters were used to acquire two 5-minute time-lapses: 800 nm excitation; unidirectional pixel scanning rate at 2 μs/pixel; 255×255 μm^2 field of view (FOV); 256×256 matrix; 2.33 Hz framerate; 700 repetitions. Each FOV was acquired twice, once at rest and once during visual stimulation. Imaging was performed at two different regions in each mouse, per imaging session, and the same FOVs were re-imaged at the subsequent 2 imaging session. Thus, in total, there were 14 pial arterioles imaged in the dataset of cohort 1. They were imaged 6 times (3 times at rest, 3 times with different frequencies of visual stimulation). Visual stimulation was performed using a computer screen (19", Acer) that was placed in the left visual field of the mouse, on which a checkerboard (2×2 cm white and black squares) was flashing at 5 Hz. The visual stimulation additionally contained an enveloping frequency, during which it was on (flashing at 5 Hz), or off. Three different enveloping frequencies were used, which were centered around the vasomotion frequency:

- 10 imaging frames on/10 frames off (4.3 seconds (s) on/4.3 s off, 0.12 Hz)
- 20 frames on/20 frames off (8.6 s on/8.6 s off, 0.06 Hz)
- 40 frames on/40 frames off (17.2 s on/17.2 s off, 0.03 Hz)

The visual stimulation paradigm lasted for the duration of one 5-minute time-lapse, and during the "off" durations of the paradigm, the computer screen displayed a grey screen. A custom-made black piece of fabric was placed between the objective and the head of the mouse to shield the light from the computer screen entering the objective and held in place with black light-tight tape. Every arteriole underwent all the three types of visual stimulation paradigms once, at separate imaging sessions, where the order of the displayed frequency was random. To confirm that the identification of arterioles was done correctly, line scans were acquired (for 2.5 s at 4.1 kHz frame rate and 0.331 μm pixel size) in 13 of the 14 vessels, as well as in 13 vessels that were assumed to be venules, to measure red blood cell velocity, as previously described.[24] Indeed, the red blood cell velocity was higher in all vessels that were classified as arterioles (supplementary figure 1), confirming our visual identification was correct.

In the second cohort of mice, 13 different pial arterioles were imaged using the same microscope as in cohort 1, with the same settings, except for the following: the mice were injected with 70 kDa Texas red-labeled dextran i.v. instead of fluorescein-labeled dextran, to allow for GCaMP imaging in a separate channel than the vessels; 2-photon excitation was performed at 900 nm instead of 800 nm for imaging of both GCaMP and Texas red at the same time; the field of view was increased to 510×510 μm^2, but with the same matrix size, thus leading to a twofold increase in pixel size. All vessels were imaged at rest, two vessels were imaged twice, and in one of the vessels, an extra time-lapse was acquired while the mouse was subjected to 0.05 Hz whisker stimulation. The stimulation was done with a T-shaped wooden rod moving up and down at 4 Hz, while the rod movement was initiated using a servo coupled to an Arduino.

Image processing

Images in the timelapses were first aligned with translation-only registration, using the imwarp function in the MATLAB Image Processing Toolbox (version 2017a, Mathworks, USA). Thereafter, a pixel timing correction was applied, because pixels within 1 image were acquired at different times (note that at our framerate, there is a ~429 ms timing difference between the first and last acquired pixel), explained in more detail in.[25] The correction was done using linear interpolation of each pixel value over time, where the timing of the first acquired pixel in each image was the reference time. One dataset was acquired with different pixel readout directions (parallel or perpendicular to the vessel orientation), and different framerates, to test the robustness of the pixel timing correction (supplementary figure 2A). Indeed, the correction successfully removed biases introduced by the different pixel acquisition times (supplementary figure 2B).

Subsequently, for cross-correlation analysis (see below), regions of interest (ROIs) were manually drawn perpendicular to the arterioles in all the datasets, using the line tool in the software ImageJ (National Institutes of Health, Bethesda, Maryland, USA). Each line-ROI was spaced 15 µm from the next line-ROI, as seen from the middle of the vessel, and the line-ROIs were drawn along the full length of the arteriole, see Figure 3 for an example. Thereafter, the line-ROIs were imported into MATLAB and the vessel diameter was estimated at each line-ROI using an in-house developed MATLAB script. Since single line signal profiles often gave a noisy vessel diameter output, a pre-processing step was performed to increase the signal to noise ratio (SNR). First, 10 additional lines were automatically created next to each hand drawn line-ROI: 5 lines to the left and 5 lines to the right of the hand drawn line-ROI, all with the same length and spaced 1 pixel apart from each other. Subsequently, line signal profiles were retrieved for all 11 lines and averaged into 1 signal profile. The vessel diameter was then calculated by estimating the full width at half maximum (FWHM) of this averaged signal profile. For the calcium signal, the same line-ROIs as for the vessel diameter calculations were used. However, in this case, the lines were converted into boxes with the same length as the line-ROI, and a width of 7 pixels. The local calcium signal was then calculated by averaging the signal of all the pixels in the box.

For the averaged vessel responses in Figure 2(a), an adapted demeaning method was applied. It was observed that different frequencies of stimulation led to similar durations of the vessel response (around 5 seconds before returning back to baseline, see Figure 2(a)). Thus, subtracting the mean diameter for each diameter time-profile, to compare the magnitude of the vessel response between different stimulation frequencies, may introduce bias in the results, given that at higher frequencies, response durations are relatively longer. Therefore, to better compare the magnitude of the vessel responses for the different visual stimulation frequencies in Figure 2(a), the diameter time-profiles were first normalized to the corresponding averaged diameter measured in the resting state time-lapse (acquired just before the time-lapse with visual stimulation). For the spectral density plots in Figures 1 and 2, MATLAB's fft function was used.

To estimate if there was propagation of vessel diameter change or calcium signaling along the pial arteriole, cross-correlation was performed between the retrieved diameter/calcium time-profiles, using an in-house developed MATLAB script and the chronux MATLAB library (http://chronux.org/). In this script, the time profile was first demeaned, detrended (using 60 knots) to remove any drift in the data, and low-pass filtered (<0.2 Hz) to remove any non-vasomotion/non-visual stimulus related higher frequency fluctuations. See supplementary figure 3 for the effect of these processing steps on the raw diameter time-profiles. Then, a reference ROI was chosen for each dataset, usually the most distal ROI, but sometimes 1 or 2 ROIs more towards the center from the most distal ROI if the time profile in the most distal ROI was noisier than the others. The time profiles for all ROIs were then cross-correlated to the reference ROI using the xcorr MATLAB function. Time-lags were retrieved for every ROI, and a linear correlation was performed between the ROIs distance from the reference ROI and their time-lags, to determine if there was significant propagation along the arteriole. Additionally, the demeaned, detrended and filtered diameter time-profiles were used to estimate total vessel diameter change, by calculating the area under the curve (AUC) for each ROI and averaging them per vessel.

Statistics

All statistical testing was done using non-parametric tests, given that the data was not always normally distributed. Shapiro-Wilk tests were used to test for normality. To test if vessel diameter changes were significantly different between datasets acquired at resting state and those acquired during visual stimulation, a paired Wilcoxon signed rank test was applied. To test if there was an effect of the different stimulation frequencies (0.12 Hz, 0.06 Hz, 0.03 Hz), a paired Friedman test was applied. To test if vasomotion wave speeds were different between resting state and visual stimulation datasets, non-paired tests were applied because of
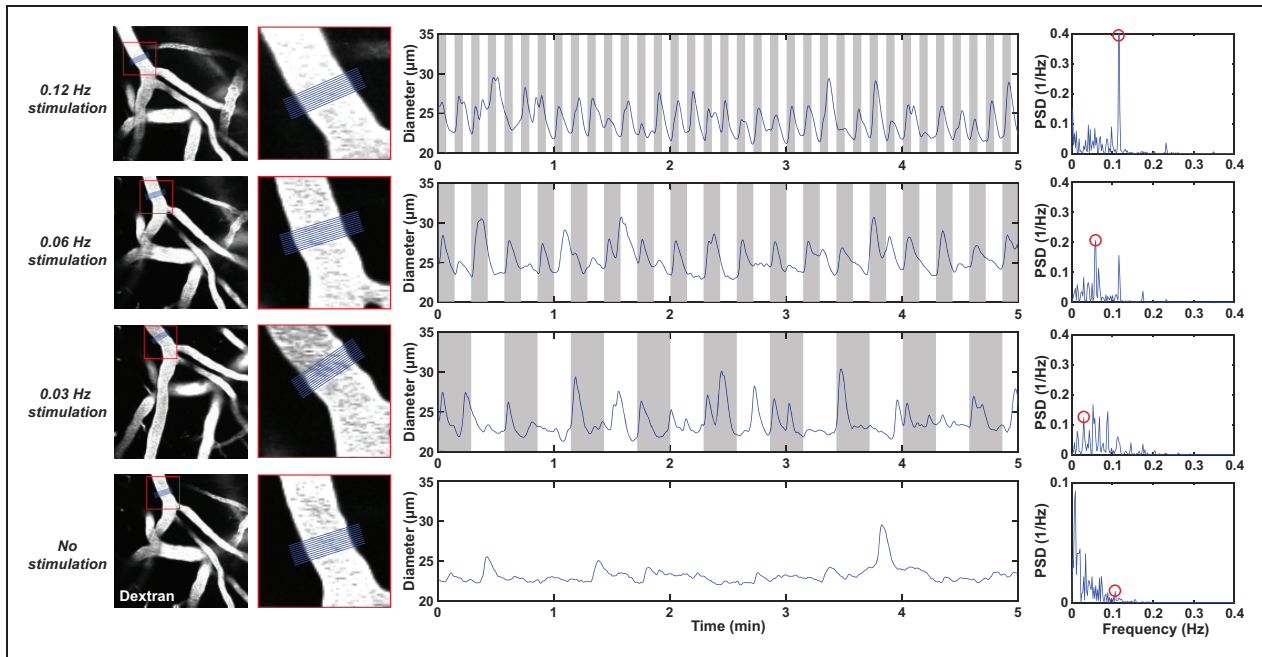
Figure 1. Examples of diameter time profiles measured in one pial arteriole with different frequencies of visual stimulation. The rows represent the different frequencies (0.12, 0.06, 0.03 Hz or no stimulation, from top to bottom). The images in the left column show the example arteriole, where the red square highlights a region that is shown at higher magnification in the second column from the left. In blue, the region of interest (ROI) is shown where the diameter was measured. The middle column shows the diameter time-profiles measured in the blue ROI; the grey areas show when the checkerboard was on. In the right column, the data of the middle column is displayed in the frequency domain. Note the respective peaks at the stimulation frequencies, highlighted in red circles. The vasomotion peak is highlighted for the resting state example. Note the different y-axis scaling in the resting state spectral plot.

missing values. Thus, a Mann Whitney U test was applied to test if there were differences between resting state and visual stimulation, and a Kruskall Wallis test for effects of the different stimulation frequencies. The statistical tests were performed in the statistics software package (SPSS), version 22 (IBM, Armonk, NY, USA).

Results

The amplitude of the vascular response varies with different visual stimulation frequencies

We first examined the individual responses of a single pial arteriole to different visual stimulation frequencies (0.12 Hz, 0.06 Hz, 0.03 Hz or no visual stimulation) in an awake head fixed C57Bl/6J mouse (Figure 1). The gray area in the plots indicates when the flashing checkerboard was on. Vessel diameters consistently increased when the checkerboard was turned on. Furthermore, in the spectral plots, peaks can be observed at the respective stimulation frequencies, while in the resting state data, a smaller peak is seen around the vasomotion frequency (0.1 Hz).

Subsequently, we averaged and normalized vascular responses averaged over all vessels (n = 14 arterioles), all ROIs, and all stimulation repeats (Figure 2(a)). Lower stimulation frequencies appeared to result in greater diameter changes: the stimulation frequencies at 0.12 Hz, 0.06 Hz, and 0.03 Hz resulted in respectively 5.2%, 8.7% and 9.1% median peak vessel diameter increases above baseline – however this was not statistically different ($\chi^2(2) = 2.67$, p = 0.264).

Next, we calculated the AUC for all demeaned, detrended and low-pass filtered time-curves (Figure 2(b)), which allows to better compare the vessel diameter changes during rest and stimulation. As expected, the total vessel diameter change was significantly higher during visual stimulation compared to rest (Z = 4.55; p < 0.001). The total vessel diameter change was highest at the 0.06 Hz stimulation frequency (42.0 at 0.06 Hz, versus 37.6 and 30.2 at 0.12 Hz and 0.03 Hz respectively), although this was not statistically significant ($\chi^2(2) = 5.17$, p = 0.076). Peaks were observed at the respective stimulation frequencies in the averaged spectral density plots (Figure 2(c)). Furthermore, in the averaged resting state spectral density plot, a smaller peak appeared around the vasomotion frequency (0.1 Hz),
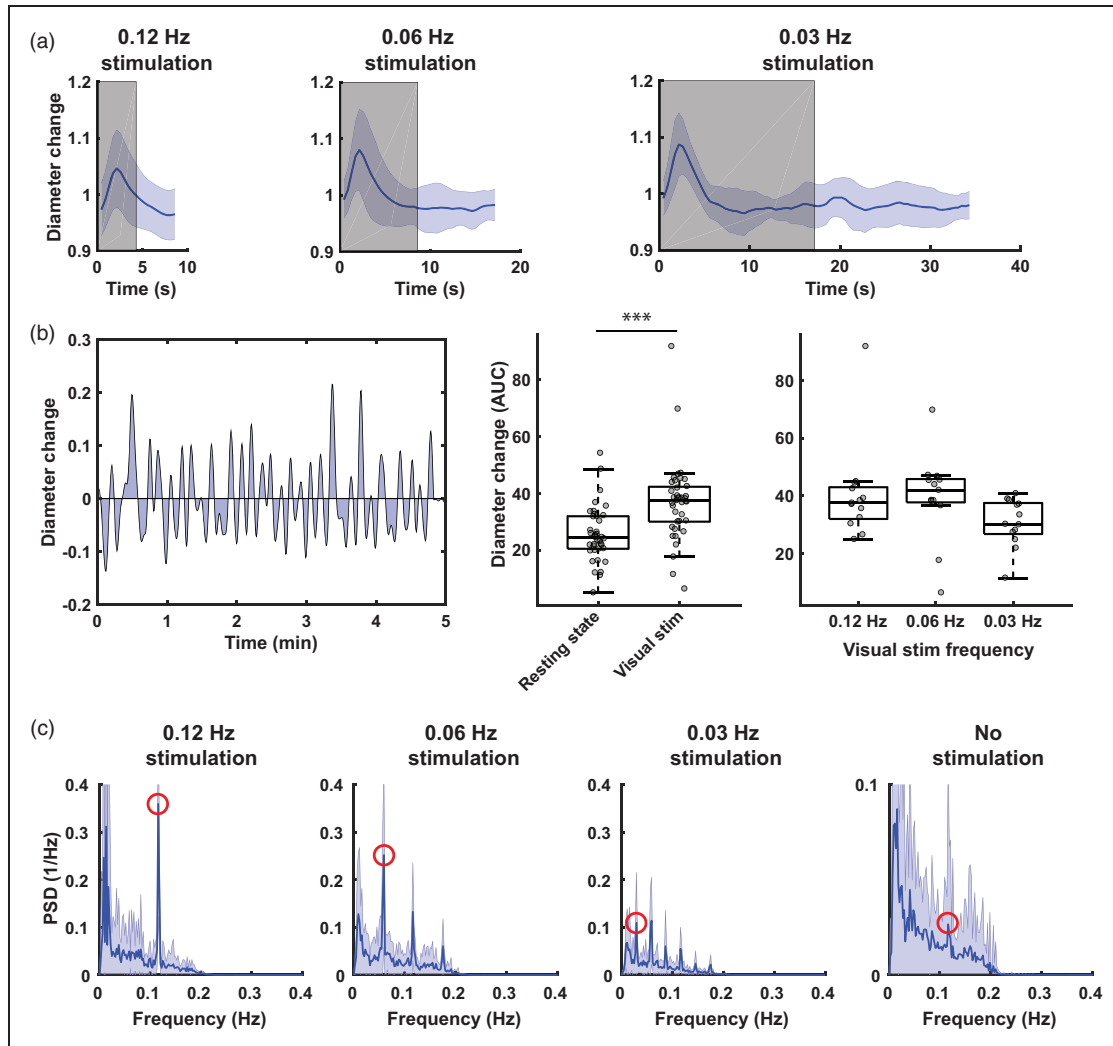
Figure 2. Group averaged responses to the different frequencies of visual stimulation. a) shows the mean (± standard deviation [SD]) of the data over all mice (n = 7, 2 vessels per mouse), all regions of interest (n =∼ 18 per vessel) and all runs (n = 34, n = 17 and n = 8 for 0.12 Hz, 0.06 Hz and 0.03 Hz respectively). The grey area indicates when the visual stimulation was on. Note the increase in peak diameter change with lower frequencies. Also note that the duration of the diameter change is approximately the same for the three frequencies. b) shows a different way of measuring the total diameter change, i.e., by calculating the area under the curve of the demeaned, detrended and low-pass filtered data. An example for one curve is shown on the left. In the middle, the area under the curve for all datasets is displayed, showing that during visual stimulation, the total diameter change is significantly higher (Mann Whitney U test, Z = 4.55, p < 0.001). On the right, the data is grouped per visual stimulation type, showing a peak diameter change at 0.06 Hz, but this was not statistically significant (Friedman, $\chi^2(2) = 5.17$, p = 0.076). On the bottom, mean (± SD) Fourier transforms are shown. Note the peaks highlighted in red at the respective stimulation frequencies, and the smaller peak at the vasomotion frequency. Also note the different y-axis scaling in the resting state plot.

which is in line with previous observations in awake mice.[15]

Vessel diameter changes propagate along pial arterioles with the same speed at rest versus during visual stimulation

We performed cross-correlation analyses to determine if vessel diameter changes propagate along pial arterioles (Figure 3). Both during visual stimulation and at rest, propagation of vessel diameter changes was observed, for which an example is shown in Figure 3(a). In supplementary figure 3, all the raw data is shown, as well as two additional examples. Additionally, for the visual stimulation datasets, the waves can be appreciated by creating an average video of the different stimulation dynamics (supplementary video 1), and further accentuated by displaying each frame as the difference from the mean frame (supplementary video 2). In 33% of the resting state datasets, significant propagation was
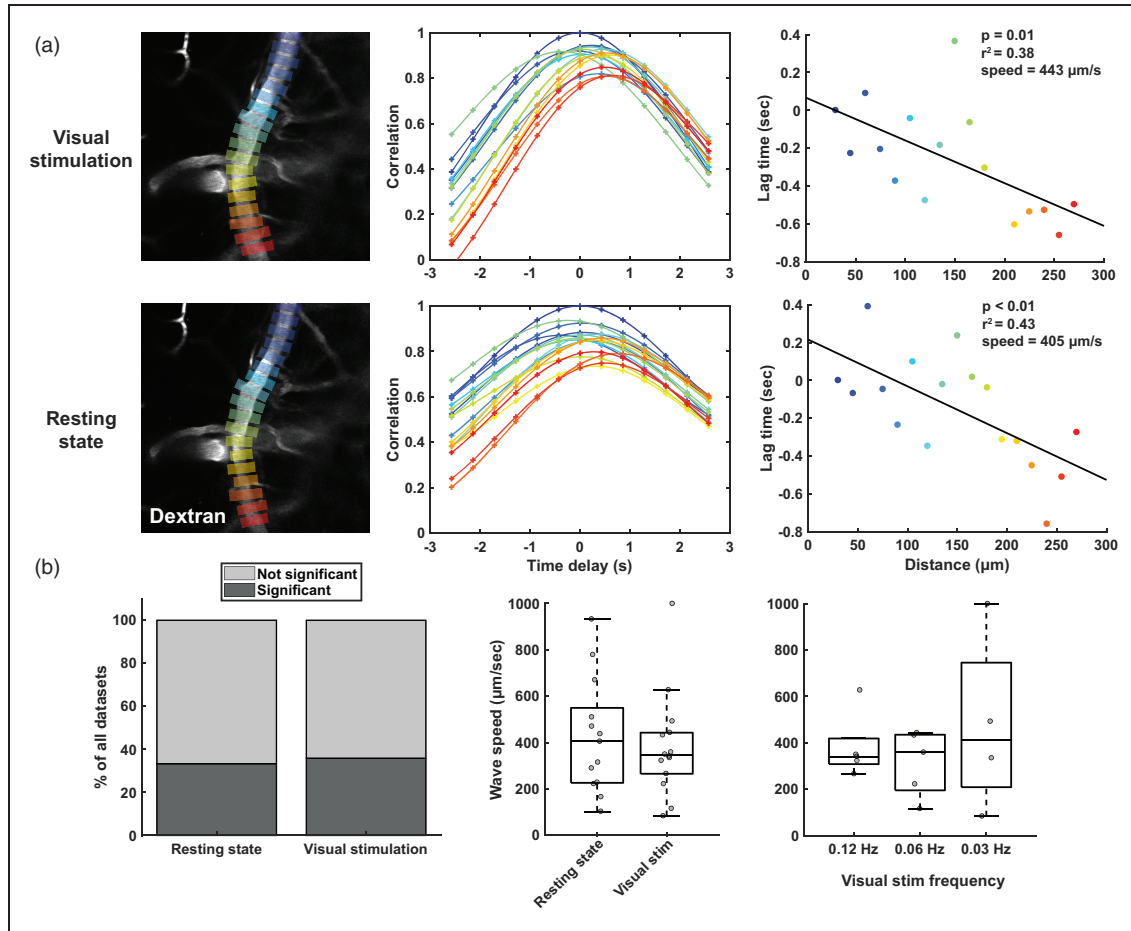
Figure 3. Detection of vessel diameter change propagation with cross-correlation analysis. a) shows an example of the cross-correlation analysis in 1 arteriole, both during visual stimulation (top row) and at rest (bottom row). In the left column, the vessel is shown with the line-ROIs, from which diameter time-profiles are retrieved for further analysis. In the middle column, the curves with different colors show the cross-correlation of the diameter time-profile from the correspondingly colored ROI on the left, with the diameter time-profile from the reference ROI on the left (dark blue one on top). Note that the further you move away from the reference ROI, the more of a shift is observed in the maximal correlation. In the right column, the distances along the vessel are plotted against the lag time retrieved from the cross-correlation peak of that ROI. Using a linear correlation, the speed of the wave is retrieved. b) shows a summary of the cross-correlation analysis of all vessels (n = 14) imaged in cohort 1 (n = 7 mice). The graph on the left shows the quantity of datasets that showed significant propagation (p-value lower than 0.05 in the linear correlation plot as in a). The two plots on the right show the wave speeds in those datasets with significant propagation, for the different conditions.

observed, which was comparable to the 36% of significant propagation in the visual stimulation datasets (Figure 3(b)). The median (interquartile range) wave speed at resting state was 405 (323) µm/s, which was comparable to the wave speed of 345 (177) µm/s during visual stimulation, ($Z = 0.32$; $p = 0.75$). The wave speeds were also similar between the different frequencies of stimulation ($\chi^2(2) = 0.52$, $p = 0.77$). The occurrence of spontaneous vasomotion waves was relatively equal across the datasets: out of the 14 arterioles in the cohort, 7 vessels showed propagation of spontaneous vasomotion at least once. Out of the 7 mice, 6 mice had at least one vessel that showed spontaneous vasomotion at least once. The majority of the waves moved against the direction of blood flow, but 1 vessel

consistently showed waves moving with the direction of blood flow (not shown).

VSMC calcium signaling propagates along pial arterioles at higher speed than vessel diameter changes

We used a second cohort of mice with GCaMP expression in their vascular smooth muscle cells (VSMCs) to investigate whether calcium signaling propagates along pial arterioles during vasomotion, like the vessel diameter changes. First, we studied calcium signal changes at the local level following sensory stimulation (note that whisker stimulation was used because of congenital blindness in the FVB background of the GCaMP
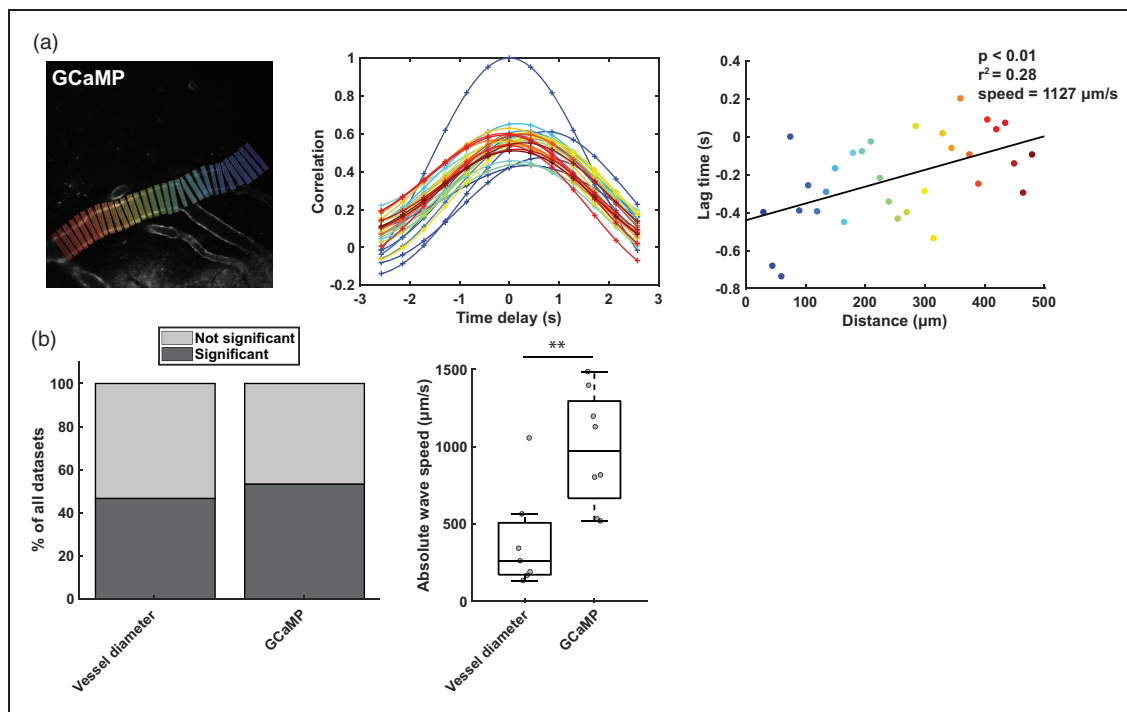
Figure 4. Detection of calcium signal propagation during resting state with cross-correlation analysis. a) shows an example of GCaMP expression in the vascular smooth muscle cells of one arteriole, and the square ROIs used to retrieve the calcium signal (average of all pixels within the square). The middle graph shows the cross-correlation of all the signals retrieved from the differently colored ROIs with respect to the reference ROI (dark blue ROI on the right). The graph on the right shows the linear correlation of the length along the arteriole and the lag time retrieved at the peak of the cross-correlation. b) shows a summary of the cross-correlation analysis of all vessels (n = 13) imaged in cohort 2 (n = 5 mice). The graph on the left shows the percentage of significant propagations observed in the vessel channel, and the percentage of significant propagations in the calcium indicator (GCaMP) channel (as shown in a). The graph on the right shows the wave speeds in those datasets with significant correlation. Note that the waves in the GCaMP channel were significantly faster than those in the vessel diameter channel (Mann-Whitney U test, Z = 2.55, p = 0.009).

mouse model). Consistent with previous reports,[26] following whisker stimulation, VSMCs calcium changes occurred before vessel diameter changes. After an initial drop in calcium concentration, the vessel diameter increased, followed by a subsequent calcium concentration increase, and a return to baseline of the vessel diameter (supplementary figure 4). Next, we used cross-correlation analysis to study the propagation of calcium signaling along the vessel tree during spontaneous vasomotion. Propagating calcium waves were observed in 53% of the datasets, with a median (interquartile range) wave speed of 972 (628) μm/s (Figure 4). Eight out 13 vessels showed propagation, of which 6 against blood flow, and 3 out of 5 mice with GCaMP expression showed spontaneous propagation of calcium signaling at least once. In supplementary figure 5, the cross-correlation analysis is also shown for the whisker stimulation dataset, together with the raw data. Surprisingly, the calcium waves and vessel diameter waves (which were imaged simultaneously in two different colors in cohort 2) were out of step: waves often occurred only in one channel, and not the other;

the calcium waves were significantly faster than the vessel diameter waves (Z = 2.55; p = 0.009); in 1 dataset, the calcium and vessel diameter waves traveled in opposite directions (supplementary figure 6). During whisker stimulation in this specific vessel, we observed that in the average response traces, the temporal shift between the calcium and vessel diameter traces changed depending on the location along the vessel (supplementary figure 4), indicating that the opposing waves are not just an artefact of the cross-correlation analysis. Despite that, vessel diameter wave speeds between cohort 1 and cohort 2 were comparable (Z = 0.55; p = 0.58).

Discussion

In this study, we first examined some basic characteristics of arteriolar diameter changes in the visual cortex of awake mice at rest and during three different frequencies of visual stimulation (0.03, 0.06, and 0.12 Hz). The total vessel displacement was higher during visual stimulation than when the mice were imaged at rest.

Furthermore, the total vessel displacement peaked around 0.06 Hz. Interestingly, this frequency is close to the frequency of spontaneous vasomotion (∼0.1 Hz).

We then used cross-correlation analyses to investigate whether diameter changes – either spontaneously occurring or evoked with visual stimulation – propagate along pial arterioles. For both spontaneous and evoked diameter changes, approximately 1 out of 3 times propagation was observed, with similar median wave speeds around 400 μm/s. Several studies have looked at wave speeds of evoked vessel diameter changes. The wave speed found here is in the same order of magnitude as the wave speed of 120 μm/s reported in Seppey et al.,[27] and 730 μm/s reported in Dietrich et al.,[28] (the latter value was extracted by dividing their average reported vessel length of 1,240 μm by the 1.7 s response time). These two studies were performed in isolated and pressurized rat arterioles. However, our reported wave speeds are considerably slower than the speed of 2,387 μm/s reported in Chen et al.,[8] which was obtained with intrinsic optical imaging in rats. Possibly, species differences as well as an underestimation on our end due to a lower framerate (and hence missing the faster waves), could explain the discrepancy in these outcomes. Notably, these studies measured propagation of evoked vessel diameter changes, whereas here we also performed measurements in spontaneously occurring vessel diameter changes. Previous studies have linked spontaneous vasomotion to changes in neural activity.[12,29] These changes could be related to the low frequency envelope occurring over gamma band activity during rest.[12] However, low frequency spontaneous motor actions such as body movement or whisking have also been shown to be accompanied by neural activity changes in sensory and motor regions.[30] The spontaneous vessel diameter changes observed here are therefore likely spontaneous occurrences of functional hyperemia, and thus it is to be expected that its propagation properties are similar to visually-evoked functional hyperemia. This also indicates that the same hemodynamic response functions can be used to model signal changes in stimulus-evoked and resting-state fMRI data.

Given the intricate link between the calcium concentration within the VSMC and its contractility, we hypothesized that the change in vessel diameter waves would be preceded by similar VSMC calcium waves. We thus used a second cohort of mice with GCaMP expression in their VSMCs, to visualize calcium signaling in pial arterioles. On the local level, vessel diameter changes were indeed coupled to calcium concentration changes. Furthermore, calcium concentration changes propagated along the vascular tree. Somewhat surprisingly, the calcium wave speeds were significantly faster than the diameter wave speeds. By studying local time

delays between calcium concentration changes and vessel diameter changes, we observed that the time delay between changes in calcium concentration and diameter differs locally along the arteriole. This confirms that the different speeds between the calcium and vessel diameter waves are related to these local timing differences, and not decoupling of calcium concentration and vessel diameter altogether. The difference in speed is also in line with data of Rungta et al.,[7] who showed that propagation of calcium concentration changes from penetrating arterioles to pial arterioles was faster than propagation of vessel diameter changes. Lastly, in one dataset we observed an opposing direction of the calcium and diameter waves. This might be related to the origin of the signal to regain vascular tone. Since this signal originates in larger arteries, by adrenergic signaling through receptors that are specifically expressed in larger arteries,[31] this gives rise to a second calcium wave, in the opposite direction and with opposite polarity of the first wave. Possibly, the cross-correlation analysis was more sensitive to the opposite calcium wave in this dataset. In short, our data confirms the existence of spontaneous calcium waves in the VSMCs, but also shows that there are local differences in how fast calcium concentration changes lead to changes in vessel diameter.

Propagation of vasomotion waves from the parenchyma up towards the brain surface, against the direction of blood flow, is a prerequisite for the brain clearance model of Aldea et al.[21] In this model, the basement membrane within the vessel wall is assumed to be fluid-filled and compressible. Consequently, outward traveling vasomotion waves would peristaltically pump waste-containing fluid through the vascular basement membrane out of the brain. Indeed, we found that vasomotion propagated along pial arterioles, and mostly against the direction of blood flow. However, it should be stressed that here, we studied pial arterioles, not penetrating cortical arterioles, so it should be confirmed in future studies whether penetrating arterioles show similar propagation. Furthermore, the compatibility of the vascular basement membrane itself with the proposed flow is questionable, since gaps in between the sheets of mural cells [32] would get rid of the required pressure difference. Alternatively, this peristaltic model could be applied to the perivascular space (PVS) itself. In this case, an outward traveling vasomotion wave would pump waste-containing fluid from the PVS around penetrating arterioles to the PVS around pial arterioles. The higher resistance from the brain tissue and the lower resistance from the pial PVS (due to its larger size[33]), would indeed create the required pressure difference. In such a peristaltic pumping model, resistance and compliance should be added as boundary conditions, given that their

inclusion in models of cardiac effects on CSF flow has shown to generate models that better reflect *in vivo* observations.[34] Interaction of the vasomotion wave with compliant brain tissue should also be considered, which would result in brain tissue deformations with pressure changes in the PVS.[35]

An interesting area for future research is vasomotion in penetrating arterioles, where the peristaltic pumping of waste-containing fluid is supposed to take place. However, this would require a more advanced technical set-up (such as a microscope that allows for X-Z scanning). Nevertheless, it is interesting to point out that for both cohorts of mice, we found that most waves were propagating against the direction of blood flow. It thus seems likely that the waves we observed indeed originated in smaller vessels in the tissue and propagated through the penetrating arterioles upwards to the brain surface. Furthermore, future studies could also look at whether the waste-containing fluid in the PVS itself shows significant propagation during a vasomotion wave, for example with fluorescent particle tracing in the PVS. Previous *in vivo* studies have generally observed movement of tracers from the subarachnoid space along the arterial tree into rather than out of the brain however.[18,36,37] Lastly, it would be of interest to study if the dynamics of vasomotion wave propagation change with diseases such as CAA.

A limitation of this study is the low sampling rate, as well as different pixel sampling times within one image. Possibly, this prevented us from imaging faster waves, and might thus have led to an underestimation of the occurrence and speed of vasomotion waves. Using a faster microscope for a future study would reduce this drawback. Alternatively, one could increase the FOV to increase the upper limit of wave speeds that can be imaged. This would also allow to study how vasomotion propagates through a network of vessels, an important topic that needs to be further explored. However, a larger FOV might make it more difficult to detect vasomotion waves, as the same FOV could contain two waves originating in different brain areas. Another limitation is that we performed a craniotomy. Even though we waited three weeks between surgery and imaging, the craniotomy may have impacted normal vascular physiology. Moreover, we cannot completely rule out that the brief isoflurane exposure at the start of the experiment to allow i.v. administration of dextran may have been a potential source of bias affecting our hemodynamic measurements. Lastly, this study was performed in awake mice, while brain clearance is thought to be predominantly occurring during sleep.[38] Future studies could therefore employ imaging techniques that can penetrate through the skull, or use a thinned skull preparation, as well as focus on imaging methods that can be performed while the animal is asleep.

In conclusion, in this study we show that, despite its lower amplitude, spontaneous vasomotion propagates along pial arterioles like stimulus-evoked vascular reactivity. This is important to consider when modeling perivascular soluble waste clearance, which is implicated in pathologic protein accumulation in neurodegenerative disease.

Declaration of conflicting interests

The author(s) declared no potential conflicts of interest with respect to the research, authorship, and/or publication of this article.

Authors' contributions

LPM and SJvV set up the study design; LPM, OB, MGK, SSH and SJvV contributed to data acquisition; LPM, OB, CAA, LH and SSH performed data analysis; LPM, MGK, SMG, BJB and SJvV helped with the interpretation of the data, LPM and SJvV drafted the article.

ORCID iDs

Leon P Munting https://orcid.org/0000-0002-2352-4451
Orla Bonnar https://orcid.org/0000-0002-8665-558X
Lydiane Hirschler https://orcid.org/0000-0003-2379-0861
Susanne J van Veluw https://orcid.org/0000-0002-7957-8643

Supplementary material

Supplemental material for this article is available online.

References

1. Iadecola C. The neurovascular unit coming of age: a journey through neurovascular coupling in health and disease. *Neuron* 2017; 96: 17–42.
2. Logothetis NK and Pfeuffer J. On the nature of the BOLD fMRI contrast mechanism. *Magn Reson Imaging* 2004; 22: 1517–1531.

3. Ma Y, Shaik MA, Kim SH, et al. Wide-field optical mapping of neural activity and brain haemodynamics: considerations and novel approaches. *Philos Trans R Soc Lond B Biol Sci* 371: 20150360.

4. Sharma R and Sharma A. Physiological basis and image processing in functional magnetic resonance imaging: neuronal and motor activity in brain. *Biomed Eng Online* 12: 113.

5. Longden TA, Hill-Eubanks DC and Nelson MT. Ion channel networks in the control of cerebral blood flow. *J Cereb Blood Flow Metab* 2016; 36: 492–512.

6. Iadecola C, Yang G, Ebner TJ, et al. Local and propagated vascular responses evoked by focal synaptic activity in cerebellar cortex. *J Neurophysiol* 1997; 78: 651–659.

7. Rungta RL, Chaigneau E, Osmanski BF, et al. Vascular compartmentalization of functional hyperemia from the synapse to the pia. *Neuron* 2018; 99: 362–375.e4.

8. Chen BR, Bouchard MB, McCaslin AFH, et al. High-speed vascular dynamics of the hemodynamic response. *Neuroimage* 2011; 54: 1021–1030.

9. Tian P, Teng IC, May LD, et al. Cortical depth-specific microvascular dilation underlies laminar differences in blood oxygenation level-dependent functional MRI signal. *Proc Natl Acad Sci U S A* 2010; 107: 15246–15251.

10. Haddock RE and Hill CE. Rhythmicity in arterial smooth muscle. *J Physiol* 2005; 566: 645–656.

11. Haddock RE, Hirst GDS and Hill CE. Voltage independence of vasomotion in isolated irideal arterioles of the rat. *J Physiol* 2002; 540: 219–229.

12. Mateo C, Knutsen PM, Tsai PS, et al. Entrainment of arteriole vasomotor fluctuations by neural activity is a basis of blood-oxygenation-level-dependent "resting-state" connectivity. *Neuron* 2017; 96: 936–948.e3.

13. Meyer MF, Rose CJ, Hülsmann JO, et al. Impairment of cutaneous arteriolar 0.1 Hz vasomotion in diabetes. *Exp Clin Endocrinol Diabetes* 2003; 111: 104–110.

14. Nyvad J, Mazur A, Postnov DD, et al. Intravital investigation of rat mesenteric small artery tone and blood flow. *J Physiol* 2017; 595: 5037–5053.

15. van Veluw SJ, Hou SS, Calvo-Rodriguez M, et al. Vasomotion as a driving force for paravascular clearance in the awake mouse brain. *Neuron* 2020; 105: 549–561.e5.

16. Rayshubskiy A, Wojtasiewicz TJ, Mikell CB, et al. Direct, intraoperative observation of ∼0.1 Hz hemodynamic oscillations in awake human cortex: implications for fMRI. *Neuroimage* 2014; 87: 323–331.

17. Kiviniemi V, Wang X, Korhonen V, et al. Ultra-fast magnetic resonance encephalography of physiological brain activity-glymphatic pulsation mechanisms? *J Cereb Blood Flow Metab* 2016; 36: 1033–1045.

18. Mestre H, Tithof J, Du T, et al. Flow of cerebrospinal fluid is driven by arterial pulsations and is reduced in hypertension. *Nat Commun* 2018; 9: 4878.

19. Iliff JJ, Wang M, Liao Y, et al. A paravascular pathway facilitates CSF flow through the brain parenchyma and the clearance of interstitial solutes, including amyloid β. *Sci Transl Med* 2012; 4: 147ra111–ra111.

20. Greenberg SM, Bacskai BJ, Hernandez-Guillamon M, et al. Cerebral amyloid angiopathy and Alzheimer disease – one peptide, two pathways. *Nat Rev Neurol* 2020; 16: 30–42.

21. Aldea R, Weller R, Wilcock D, et al. Cerebrovascular smooth muscle cells as the drivers of intramural periarterial drainage of the brain. *Front Aging Neurosci* 2019; 11: 1.

22. Cuttler AS, Leclair RJ, Stohn JP, et al. Characterization of Pdgfrb-Cre transgenic mice reveals reduction of ROSA26 reporter activity in remodeling arteries. *Genesis* 2011; 49: 673–680.

23. Kilkenny C, Browne WJ, Cuthill IC, et al. Improving bioscience research reporting: the ARRIVE guidelines for reporting animal research. *PLoS Biol* 2010; 8: e1000412.

24. Arbel-Ornath M, Hudry E, Eikermann-Haerter K, et al. Interstitial fluid drainage is impaired in ischemic stroke and Alzheimer's disease mouse models. *Acta Neuropathol* 2013; 126: 353–364.

25. Boiroux D, Oke Y, Miwakeichi F, et al. Pixel timing correction in time-lapsed calcium imaging using point scanning microscopy. *J Neurosci Methods* 2014; 237: 60–68.

26. Hill RA, Tong L, Yuan P, et al. Regional blood flow in the normal and ischemic brain is controlled by arteriolar smooth muscle cell contractility and not by capillary pericytes. *Neuron* 2015; 87: 95–110.

27. Seppey D, Sauser R, Koenigsberger M, et al. Intercellular calcium waves are associated with the propagation of vasomotion along arterial strips. *Am J Physiol Heart Circ Physiol* 2010; 298: 488–496.

28. Dietrich HH, Horiuchi T, Xiang C, et al. Mechanism of ATP-induced local and conducted vasomotor responses in isolated rat cerebral penetrating arterioles. *J Vasc Res* 2009; 46: 253–264.

29. Ma Y, Shaik MA, Kozberg MG, et al. Resting-state hemodynamics are spatiotemporally coupled to synchronized and symmetric neural activity in excitatory neurons. *Proc Natl Acad Sci U S A* 2016; 113: E8463–E8471. E8471.

30. Drew PJ, Winder AT and Zhang Q. Twitches, blinks, and fidgets: important generators of ongoing neural activity. *Neuroscientist* 2019; 25: 298–313.

31. Koep JL, Taylor CE, Coombes JS, et al. Autonomic control of cerebral blood flow: fundamental comparisons between peripheral and cerebrovascular circulations in humans. *J Physiol* 2022; 600: 15–39.

32. Pizzo ME, Wolak DJ, Kumar NN, et al. Intrathecal antibody distribution in the rat brain: surface diffusion, perivascular transport and osmotic enhancement of delivery. *J Physiol* 2018; 596: 445–475.

33. Bedussi B, Almasian M, de Vos J, et al. Paravascular spaces at the brain surface: low resistance pathways for cerebrospinal fluid flow. *J Cereb Blood Flow Metab* 2018; 38: 719–726.

34. Ladrón-de-Guevara A, Shang JK, Nedergaard M, et al. Perivascular pumping in the mouse brain: Improved boundary conditions reconcile theory, simulation, and experiment. *J Theor Biol* 542: 111103.

35. Kedarasetti RT, Turner KL, Echagarruga C, et al. Functional hyperemia drives fluid exchange in the paravascular space. *Fluids Barriers CNS* August 2020; 17: 52.

36. Ringstad G, Vatnehol SAS and Eide PK. Glymphatic MRI in idiopathic normal pressure hydrocephalus. *Brain* 2017; 140: 2691–2705.

37. Iliff JJ, Lee H, Yu M, et al. Brain-wide pathway for waste clearance captured by contrast-enhanced MRI. *J Clin Invest* 2013; 123: 1299–1309.

38. Hablitz LM, Plá V, Giannetto M, et al. Circadian control of brain glymphatic and lymphatic fluid flow. *Nat Commun* December 2020; 11: 4411.